Viscous effects in droplet-ejecting capillary waves

Christopher L. Goodridge,* W. Tao Shi, H. G. E. Hentschel, and Daniel P. Lathrop†
Department of Physics, Emory University, Atlanta, Georgia 30322
(Received 14 November 1996)

Surface waves produced by parametric excitation experience a transition between simply connected waves and droplet-ejecting waves when the applied forcing exceeds a threshold level. Our measurements on a number of different fluids indicate that low-viscosity fluids have threshold accelerations which depend on only surface tension and forcing frequency while high viscosity fluids have thresholds which depend on only viscosity and forcing frequency. Models for the transition based on the condition that the wavelength, waveheight ratio approaches a fixed value at the transition are consistent with our observations. [S1063-651X(97)05207-0]

PACS number(s): 47.20.Ma, 47.55.Dz, 68.10.−m, 92.10.Hm

Droplet ejection from liquid surfaces is a ubiquitous phenomenon in nature. Wave breaking on the shores and surfaces of oceans and lakes [1–3], the spray from turbulent rivers, and the splash from a raindrop hitting a puddle all involve the production of small, energetic droplets which escape and then rejoin the main body of the liquid [4–6]. This phenomenon is an important mechanism for both energy dissipation and gaseous absorption. These surface waves receive the energy needed to create droplets from sources such as the wind or gravity driven flow and require a certain minimum energy flux to produce droplets. This paper discusses the creation and characterization of droplets ejected from waves on the free surface of a liquid caused by vertically oscillating a partially filled liquid container (Faraday excitation). This allows a carefully controlled excitation of standing wave states. Both the chaotic and turbulent bifurcation behavior of Faraday surface waves have been intensively studied and many different transitions have been examined and described [7–12]. Specifically in this study, capillary waves experience a transition from a turbulent nonejecting state to a turbulent ejecting state in a number of liquids with very different fluid properties.

The transition to droplet-ejecting states in capillary surface waves is induced by increasing the applied forcing until the Rayleigh instability [13] causes wave peaks to break up into droplets. Vertically oscillated waves experience a number of bifurcations before the transition to a droplet-ejecting state [14–16]. With increasing forcing, an initially flat surface wave state will evolve into a periodic standing wave state. This then will change into an aperiodic state, which, at sufficiently large forcing, will produce large-amplitude waves, often with upward jets (or spikes) which will break into droplets [17–22]. The transition from a non-ejecting turbulent state to a state with droplet ejections is observed to be dependent on the kinematic surface tension σ/ρ and the kinematic viscosity of the fluid $\nu=\mu/\rho$, as well as the applied forcing frequency ω_0 (here ρ, σ and μ are the density, the interfacial surface tension, and the Newtonian viscosity of the liquid, respectively).

Droplet ejection in a Faraday system is a robust phenomenon. It has been observed in liquids with a two decade range in viscosity, a factor of 3 change in surface tension, and over a two decade range in frequency. Ejecting states can occur in waves where either surface tension effects or gravitational effects are the primary restoring forces. Capillary waves can be distinguished from gravity waves by using the dispersion relationship for small-amplitude, infinite depth periodic waves [23],

$$\omega^2 = gk + \frac{\sigma}{\rho}k^3, \tag{1}$$

where ω is the angular frequency of the surface waves, g the local value of the gravitational acceleration, and k the wave number of the waves. Gravitational effects and surface tension effects dominate at low and high wave number, respectively. The crossover wave number $k_c=\sqrt{g\rho/\sigma}$, where the effects are equal, determines a crossover frequency $\omega_c=g^{3/4}(\rho/\sigma)^{1/4}$. We have concentrated on the frequency region where capillary effects are the most important restoring forces ($\omega>\omega_c$). For these experiments, the wavelengths of the capillary waves are small compared to the dimensions of the container, which minimizes the effects of the container size and shape on the wave state. Parametric excitation pumps energy into waves of frequency $\omega=\omega_0/2,\omega_0,3\omega_0/2,\ldots$, with the largest amplitude at $\omega=\omega_0/2$.

We have experimentally determined the ejection threshold acceleration a dependence on the parameters ω_0, σ/ρ, and ν. Photographs in Figs. 1 and 2 illustrate the differences in droplet-ejection behavior of Faraday waves for different forcing conditions and fluid properties. Figure 1 shows the differences between low- and high-frequency droplet-ejecting waves for the fluid containers we have used. We have observed lower-frequency wave states where the states are influenced by the shape of the container [24]. Higher-frequency capillary wave states are largely independent of the container geometry and the ejecting waves are turbulent with the ejections appearing random in space and time. The effects of viscosity can be seen in Fig. 2; in low-viscosity liquids such as ethanol and water, spikes are produced which immediately break up into droplets. In high-viscosity fluids, these peaks maintain their structure and can produce long filaments before droplet breakoff occurs.

The threshold acceleration was measured for water, water-glycerin solutions, and ethanol. Fluid with a depth of

*Electronic address: cgoodri@emory.edu
†Electronic address: dpl@complex.physics.emory.edu

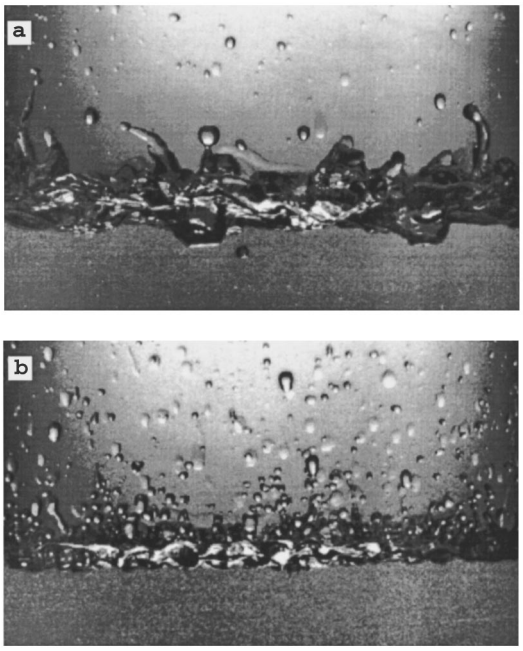

FIG. 1. Photographs show droplet-ejecting waves in distilled water at two different forcing frequencies: (a) 20 Hz and (b) 60 Hz, both show a 10 cm wide section of a 19.5 cm tank.

10 cm [25] was used in either a glass reaction flask (diameter 13.5 cm) or a cylindrical plastic container (diameter 19.5 cm). The container was then mounted on the armature of a TA100-20 Unholtz-Dikie Electromagnetic shaker which can supply a maximum force of 1100 N. A function generator

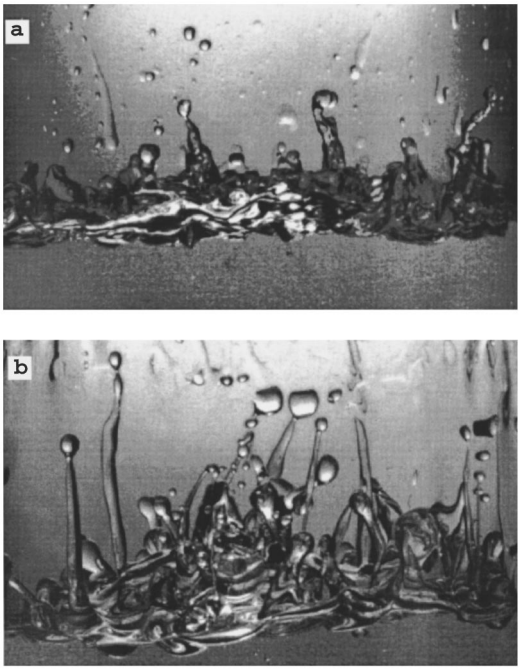

FIG. 2. Photographs of (a) distilled water ($\nu \simeq 0.01$ cm^2/s) and (b) an 80% glycerin–water solution ($\nu \simeq 0.43$cm^2 s), illustrating the different behavior at low and high viscosity. Both states are excited at 20 Hz. In distilled water, wave peaks break up into droplets almost immediately, while in the more viscous fluid, several long filamentlike peaks are visible. Both photographs show a 10 cm section of the tank.

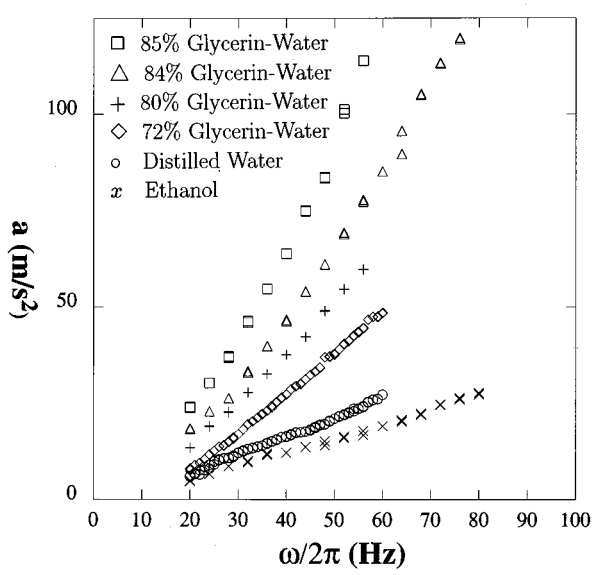

FIG. 3. Threshold acceleration for fluids of different viscosities (0.01–1.08 cm^2/s) shows the increase of the threshold acceleration with increasing viscosity.

and amplifier supplied a sinusoidal signal to the shaker. The applied acceleration was measured with an accelerometer mounted on the armature of the shaker. The accelerometer signal was processed by either fast Fourier transform (FFT) or lock-in amplifier. Temperature control was effected by using an aluminum plate as the bottom of the tank and running fluid from a constant temperature bath under the plate. The droplets were detected visually. The criterion used for onset of droplet ejection was two droplets detected within a ten second period. Such a criterion was necessary as there appears to be a critical slowing of droplet production near the threshold. This condition introduces 2–3 % error to the data. We plan to discuss the time-dependent statistical behavior and droplet production rate in a future paper.

The viscous dependence of the threshold acceleration can be seen in Fig. 3. We plot the experimental threshold acceleration a vs angular forcing frequency ω_0 scaled with the fluid parameters of kinetic surface tension σ/ρ and kinetic viscosity ν to determine the functional form of the threshold acceleration. This plot can be seen in Fig. 4. We define a nondimensional frequency [26] as

$$\omega^* = \frac{\omega_0 \nu^3}{(\sigma/\rho)^2} \tag{2}$$

and a nondimensional acceleration [26] as

$$a^* = \frac{a \nu^4}{(\sigma/\rho)^3}. \tag{3}$$

These scaled quantities display a crossover at about $\omega^* \simeq 10^{-5}$, which can be seen in Fig. 5. For $\omega^* \ll 10^{-5}$, the angular frequency dependence is observed to be $a^* \sim (\omega^*)^{4/3}$ [regression yields $(\omega^*)^{1.337}$] while for $\omega^* \gg 10^{-5}$ it shows an $a^* \sim (\omega^*)^{3/2}$ [regression yields $(\omega^*)^{1.476}$] dependence. This crossover leads to two different

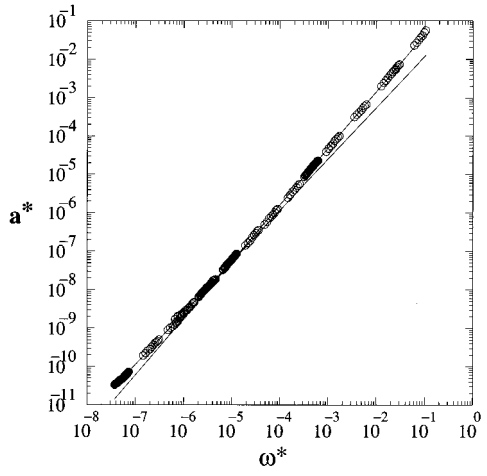

FIG. 4. Nondimensionalized acceleration $a^*=a\nu^3/(\sigma/\rho)^4$ is plotted as a function of nondimensionalized angular frequency $\omega^*=\omega_0\nu^2/(\sigma/\rho)^3$. In the lower-viscosity region ($\omega^*<10^{-5}$), we observe an $\omega_0^{4/3}$ dependence, while an $\omega_0^{3/2}$ dependence is seen in the higher-viscosity region ($\omega^*>10^{-5}$). Note also the collapse of the ethanol, water, and glycerin–distilled-water data for this nondimensionalization. The two lines are best fit to the low- and high-viscosity data, respectively.

functional forms for the threshold acceleration: for low-viscosity fluid where surface tension effects dominate the threshold acceleration a is given by

$$a\approx 0.261\left(\frac{\sigma}{\rho}\right)^{1/3}\omega_0^{4/3} \tag{4}$$

while in viscous dominated fluids, the functional form for a is

$$a\approx 1.306\nu^{1/2}\omega_0^{3/2}, \tag{5}$$

where the prefactors were determined using linear regression.

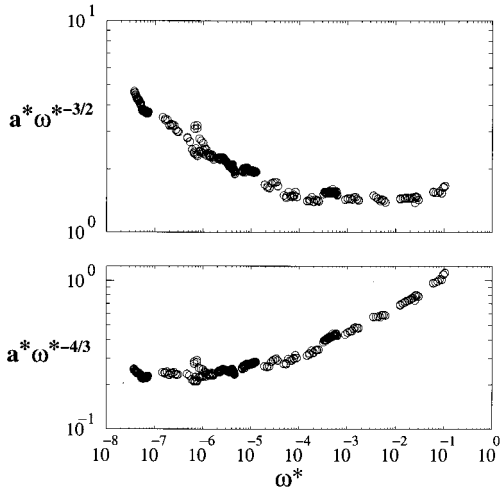

FIG. 5. Nondimensionalized acceleration is scaled with $(\omega^*)^{-3/2}$ and $(\omega^*)^{-4/3}$ to illustrate both the utility of this choice of nondimensionalization as well as the transition between high- ($\omega_0^{3/2}$) and low- ($\omega_0^{4/3}$) viscosity behavior.

Scaling arguments can be found for both regions. Models for both low-viscosity ejection and high-viscosity ejection are based on the same assumption: as the forcing is increased ejections occur when the ratio of the wave-height h to the wavelength λ approaches unity:

$$h\sim\lambda. \tag{6}$$

This assumption is supported by analytical work done on other types of fluid waves. Previous studies on traveling waves have determined limiting wave-height, wavelength ratios for both gravity and capillary waves [27,28]. These calculated ratios are $s=h/\lambda=0.14$ for gravity waves and $s=0.731$ for capillary waves. When h/λ exceeds 0.14 for gravity waves, local accelerations on the wave crest diverge, and breaking occurs. Periodic capillary waves are only possible with heights $h<0.731\lambda$. The parametric solution is self-intersecting for larger ratios. This corresponds to the impact of two diverging vertical surfaces in the wave, which may lead to jet formation [29,30] or air entrainment.

For both viscous and capillary dominated cases, we treat the motion of the tank as simple harmonic motion described by

$$z=A\sin\omega_0 t, \tag{7}$$

where z is the vertical displacement of the tank, A the peak displacement, and $\omega_0=2\omega$ the angular velocity of the external forcing. In low-viscosity situations, we shall assume that the height of the waves scales as the amplitude of the external forcing $h\propto A$ or in terms of the applied acceleration

$$h\propto\frac{a}{\omega_0^2}. \tag{8}$$

Observations confirm that $h\simeq 47a/\omega_0^2$ [31] for capillary waves. With this assumption and the dispersion relation for small-amplitude capillary waves, the threshold acceleration for droplet ejection in low-viscosity fluids scales as $a\sim h\omega_0^2\sim\lambda\omega_0^2$, or

$$a=c_1\omega_0^{4/3}\left(\frac{\sigma}{\rho}\right)^{1/3}, \tag{9}$$

where c_1 is some constant. Thus the threshold for low-viscosity fluids is dependent on only surface tension and forcing frequency [32] as is consistent with experimental observation.

In more viscous fluids, we argue that the wave height is set by the balance of power input and viscous dissipation. The viscous energy dissipation per unit mass can be written as

$$\epsilon=\sum_{i,j}\frac{\nu}{2}\left(\frac{\partial v_i}{\partial x_j}+\frac{\partial v_j}{\partial x_i}\right)^2, \tag{10}$$

where $\partial v_i/\partial x_j$ are the rate of strain components within the fluid. Energy dissipation thus scales as

$$\epsilon=\nu\left(\frac{v}{l}\right)^2, \tag{11}$$

where v and l are the characteristic length and velocity scales of the ejecting surface waves. Selecting the maximum velocity $|v_{\max}|=h\omega$ as the characteristic velocity and the wavelength λ as the characteristic length, the power dissipation becomes

$$\epsilon \simeq \nu\left(\frac{v_{\max}}{\lambda}\right)^2 = \nu\left(\frac{h\omega}{\lambda}\right)^2. \tag{12}$$

The injected power can be written in terms of the force and velocity of the tank $P=Fv$; where $v=a/\omega_0$, the peak velocity of the tank, and $F=ma$, where m is the mass of the fluid and a is the peak applied acceleration. The injected power per unit mass $p=P/m$ is thus

$$p \sim \frac{a^2}{\omega_0}. \tag{13}$$

Equating the injected power with the viscous dissipated energy and using the hypothesis $h\sim\lambda$ yields the relationship

$$a = c_2 \omega_0^{3/2} \nu^{1/2}. \tag{14}$$

Note that although the surface tension appears in the wavelength in this calculation, it drops out of the expression for the threshold acceleration for viscous liquids, as corroborated by the $a^*\sim(\omega^*)^{3/2}$ dependence of the experimental viscous observations [33].

The viscous effects on the threshold for droplet ejection in capillary Faraday waves have been explored for water, ethanol, and glycerin-water solutions. The observed viscous effects have been characterized by varying the fluid properties and the forcing parameters and determining the threshold acceleration of various fluids. A transition in the threshold behavior has been discovered and a simple scaling theory has produced relationships for both regimes of behavior, supported by our experimental observations. Future analysis of the behavior of droplet-ejecting Faraday waves will include a statistical description of the droplet rates around threshold.

The authors would like to express their gratitude to the following people: Raymond DuVarney, Michael Brown, Matthias Steffen, and Benjamin Zeff. This research was funded in part by the Emory University Research Committee.

[1] D. H. Peregrine, Annu. Rev. Fluid Mech. **15**, 149 (1983).
[2] M. L. Banner and D. H. Peregrine, Annu. Rev. Fluid Mech. **25**, 373 (1993).
[3] A. C. Newell and V. E. Zakharov, Phys. Rev. Lett. **69**, 1149 (1992).
[4] A. L. Yarin and D. A. Weiss, J. Fluid Mech. **283**, 141 (1995).
[5] M. Rein, J. Fluid Mech. **306**, 145 (1996).
[6] H. N. Oguz and A. Prosperetti, J. Fluid Mech. **294**, 181 (1995).
[7] T. B. Benjamin and F. Ursell, Proc. R. Soc. London, Ser. A **225**, 505 (1954).
[8] S. Cilberto, S. Douady, and S. Fauve, Europhys. Lett. **15**, 23 (1991).
[9] J. Miles and D. Henderson, Annu. Rev. Fluid Mech. **22**, 143 (1990).
[10] B. J. Gluckman, C. B. Arnold, and J. P. Gollub, Phys. Rev. E **51**, 1128 (1995).
[11] S. P. Decent and A. D. D. Craik, J. Fluid Mech. **293**, 237 (1995).
[12] S. Douady, J. Fluid Mech. **221**, 383 (1990).
[13] S. Chandrasekhar, *Hydrodynamic and Hydromagnetic Stability* (Dover Publications, Inc., New York, 1981).
[14] A. B. Ezerskii, P. I. Korotin, and M. I. Rabinovich, Pis'ma Zh. Éksp. Teor. Fiz. **41**, 129 (1985) [JETP Lett. **41**, 157 (1985)].
[15] N. B. Tufillaro, R. Ramshankar, and J. P. Gollub, Phys. Rev. Lett. **62**, 422 (1985).
[16] S. Ciliberto and J. Gollub, J. Fluid Mech. **158**, 381 (1985).
[17] M. S. Longuet-Higgins, J. Fluid Mech. **127**, 103 (1983).
[18] M. Tjahjadi, H. A. Stone, and J. M. Ottino, J. Fluid Mech. **243**, 297 (1992).
[19] Jens Eggers and Todd F. Dupont, J. Fluid Mech. **262**, 205 (1994).
[20] Michael Brenner, X. D. Shi, and Sidney R. Nagel, Phys. Rev. Lett. **73**, 3391 (1994).
[21] C. L. Goodridge, W. Tao Shi, and D. P. Lathrop, Phys. Rev. Lett. **76**, 1824 (1996).
[22] W. Tao Shi, C. L. Goodridge, and D. P. Lathrop (unpublished).
[23] L. D. Landau and E. M. Lifshitz, *Fluid Mechanics* (Pergamon Press, New York, 1987).
[24] In our system, lower-frequency states (waves with wavelengths comparable to the dimensions of our container) are affected by the fluid surface wave modes of the container. Roughly stationary ejecting waves as well as periodic ejecting states have been observed at very low frequencies.
[25] This depth ($d>10\lambda$) was chosen to minimize any bottom boundary contribution to the surface wave state.
[26] These nondimensional quantities can be written in terms of known groups: $\omega^*=(\mathrm{Su})^{-2/3}$ and $a^*=\mathrm{Ca}/(\mathrm{Su})^{3/2}$. The Suratman number Su is defined as $\rho l\sigma/\mu^2$ and the capillary number Ca (the ratio of viscous forces to surface tension forces) is defined as $\mu v/\sigma$, where ρ is the density, l a characteristic length, σ the surface tension, μ the Newtonian viscosity, and v a characteristic velocity.
[27] J. H. Michell, Philos. Mag. **36**, 430 (1893).
[28] G. D. Crapper, J. Fluid Mech. **2**, 532 (1957).
[29] E. Ott, Phys. Rev. Lett. **29**, 1429 (1972).
[30] J. M. Walsh, R. G. Shreffler, and F. J. Willig, J. Appl. Phys. **24**, 349 (1953).
[31] The threshold acceleration transition at $\omega^*\simeq 10^{-5}$ can be seen analytically by equating the height for low-viscosity waves ($h\simeq 47a/\omega_0^2$) with the height of high-viscosity waves ($h=a\lambda/\omega_0^{3/2}\nu^{1/2}$). With our observed low-viscosity prefactor, the transition occurs at $\omega^*\simeq 0.6\times 10^{-5}$.
[32] This expression can also be derived using simple dimensional analysis. The only dimensionally consistent way surface tension σ/ρ and frequency ω can be combined as an acceleration a is $a\propto(\sigma/\rho)^{1/3}\omega^{4/3}$.
[33] The only dimensionally consistent way $\omega^{3/2}$, ν, and σ/ρ can be combined to form an acceleration is $a=\omega^{3/2}\nu^{1/2}$.